

2021-12

Global syndromes induced by changes in solutes of the world's large rivers

Wu, J

<http://hdl.handle.net/10026.1/18291>

10.1038/s41467-021-26231-w

Nature Communications

Springer Science and Business Media LLC

All content in PEARL is protected by copyright law. Author manuscripts are made available in accordance with publisher policies. Please cite only the published version using the details provided on the item record or document. In the absence of an open licence (e.g. Creative Commons), permissions for further reuse of content should be sought from the publisher or author.

1 **Supplementary Information for**

2
3 **Global syndromes induced by changes in solutes of the world's large rivers**

4 Jiang Wu^{1,2,8}, Nan Xu^{2,8}, Yichu Wang³, Wei Zhang⁴, Alistair G.L. Borthwick^{5,6}, Jinren
5 Ni^{1,7*}

6
7 ¹State Environmental Protection Key Laboratory of All Materials Fluxes in River
8 Ecosystems, Peking University, Beijing 100871, P. R. China;

9 ²The Key Laboratory for Heavy Metal Pollution Control and Reutilization, School of
10 Environment and Energy, Peking University Shenzhen Graduate School, Shenzhen
11 518055, P. R. China;

12 ³College of Water Sciences, Beijing Normal University, Beijing 100875, P. R. China;

13 ⁴Department of Plant, Soil and Microbial Sciences, Michigan State University, East
14 Lansing, MI 48824, United States;

15 ⁵Institute of Infrastructure and Environment, School of Engineering, The University of
16 Edinburgh, The King's Buildings, Edinburgh EH9 3JL, UK;

17 ⁶School of Engineering, Computing and Mathematics, University of Plymouth, Drake
18 Circus 14 Plymouth, PL4 8AA, UK;

19 ⁷Center for Global Large Rivers, School of Environmental Science and Engineering,
20 Southern University of Science and Technology, Shenzhen 518055, P. R. China.

21 ⁸These authors contributed equally: Jiang Wu, Nan Xu

22

23

24 *Correspondence and requests for materials should be addressed to J.R.N.

25 (jinrenni@pku.edu.cn).

26

27 **This PDF file includes:**

28

29 Supplementary Methods

30 Supplementary Figs. 1 to 10

31 Supplementary Tables 1 to 9

32 Supplementary References 1 to 87

33 **Supplementary Methods**

34 **1. Database compilation**

35 To construct a global database of major dissolved ions in the world's large rivers (\geq
36 1,000 km²)¹, we compiled information from 12 publicly available databases (listed in
37 Supplementary Table 7) and also extracted long-term hydrochemical data from the open
38 literature²⁻³⁷.

39 We consolidated these data in a global dataset of major dissolved ions and total
40 dissolved solids (TDS) in the world's large rivers. First, we combined all the data from
41 all our sources. Then, for any overlapping data at any given station in any given year,
42 if the difference was less than 10%, we calculated the average of all reported data from
43 all the databases. If the discrepancy was greater than 10%, we used expert judgement
44 and usually preserved the value from whichever record was the longer. Annual average
45 concentrations of 8 major dissolved ions (Ca²⁺, Mg²⁺, Na⁺, K⁺, SO₄²⁻, Cl⁻, HCO₃⁻ and
46 dissolved silica (DSi)) were calculated by averaging measured values at finer time steps
47 (monthly or seasonally) whenever available. Otherwise, average annual concentrations
48 were taken from values reported in the literature. In cases where TDS data were already
49 available in the data sources, we used these records. In cases of any missing TDS
50 measurements, we simply summed the concentrations of all DS (Ca²⁺, Mg²⁺, Na⁺, K⁺,
51 SO₄²⁻, Cl⁻, HCO₃⁻ and DSi) to determine TDS when all the DS values were available.
52 For the TDS data, we obtained 8,016 data points directly from open databases, 485 data
53 points from model results (explained in more detail in Section 2, Supplementary
54 Methods), 121 data points from the literature, and 543 data points by summing the

55 concentrations of all dissolved ions. Thus, about 87% of the TDS data were taken
56 directly from public databases.

57 In addition to the global database of TDS, we also compiled the annual average flows
58 of the world's large rivers in the PKU-IEE-WLRs-WS-NL2006 Database.
59 Supplementary Table 8 lists the source databases for the annual river discharge data.
60 Any missing data were filled by river discharge data taken from the literature and online
61 sources²⁻³⁷. We consolidated all the river discharge data using an approach similar to
62 that for the dissolved solids database, particularly overlapping data.

63 In summary, our database includes data from 600 stations in 149 rivers located across
64 six continents, as shown in Fig. 1 of the main text. The stations are distributed as follows:
65 54.8% in North America, 14.8% in Asia, 12.2% in Oceania, 8.2% in Europe, 7.5% in
66 South America, and 2.5% in Africa. The percentage of stations with records no less than
67 5 years ranged between 82-86% for all DS. Moreover, 43–52% of stations had records
68 of duration 10-30 years for 8 major dissolved ions and TDS (Supplementary Table 9).
69 To our knowledge, this database is the most comprehensive to date in terms of spatial
70 and temporal coverage of DS.

71 **2. Data quality**

72 **2.1 Outlier detection**

73 To control data quality (and ensure robust trend analysis and flux calculations), we
74 removed outliers in the database, as is usual practice³⁸. First, we tested whether the time
75 series data for any of DS at any given station followed a normal distribution. If so, then
76 outliers were identified using the Grubbs' test³⁹ using the R package 'outliers'. If not,

77 any data points beyond three standard deviations (SD) of the mean⁴⁰ were considered
78 outliers. We removed 1,273 outliers using the Grubbs' test and 615 outliers using the
79 three SD method. The percentage number of removed outliers was 2.3% of the total
80 data points.

81 **2.2 Charge balance**

82 We selected 6,124 annual average concentration data samples containing all major
83 charged ions ($\text{Ca}^{2+}/\text{Mg}^{2+}/\text{Na}^+/\text{K}^+/\text{SO}_4^{2-}/\text{Cl}^-/\text{HCO}_3^-$) to assess data quality using the
84 charge balance approach (in meq = 10^{-3} equivalents per liter). This method compared
85 the total charge carried by total dissolved cations ($\text{TZ}^+ = \text{Na}^+ + \text{K}^+ + 2\text{Mg}^{2+} + 2\text{Ca}^{2+}$) to
86 that by total dissolved anions ($\text{TZ}^- = \text{Cl}^- + \text{HCO}_3^- + 2\text{SO}_4^{2-}$). Given that all dissolved
87 ions in water should retain total neutrality, the normalized inorganic charge balance
88 ($\text{NICB} = (\text{TZ}^+ - \text{TZ}^-)/(\text{TZ}^+ + \text{TZ}^-) \times 100\%$)^{31, 41} should be less than 10% on average.
89 In our database, 5,447 annual average data (89%) met this criterion, indicating high
90 data quality (within the usual combined analytical uncertainty for all measurements^{6,}
91 ⁴²).

92 **3. Flux calculation**

93 To calculate the annual fluxes of DS in the world's large rivers, we used a hybrid
94 approach that utilized observed annual concentrations and river flows for direct
95 calculation supplemented with LOAD ESTimator model results for any missing data.
96 The direct calculation and modeling methods are described below.

97 **3.1 Direct calculation**

98 Solute flux was calculated as the product of annual average concentrations (C_i) and

99 annual average flow (Q_i) as follows:

$$100 \quad F_{\text{ea}} = k \times C_i \times Q_i \quad (\text{S1})$$

101 where $k = 0.001$ is the conversion coefficient, F_{ea} is the annual flux, C_i is the annual
102 average concentration of Ca^{2+} , Mg^{2+} , Na^+ , K^+ , SO_4^{2-} , Cl^- , HCO_3^- , and DSi , and Q_i is
103 the annual average flow for a given year at a specific station.

104 **3.2 LOADEST Model**

105 For any undocumented (or missing) data, we used the LOAD ESTimator
106 (LOADEST), a FORTRAN program for estimating constituent loads in streams and
107 rivers based on daily runoff data and calibrated concentrations⁴³, to estimate any
108 missing annual flux values the direct method could not calculate. Adjusted Maximum
109 Likelihood Estimation (AMLE) was used to fit the calibration equation. Then the
110 regression model with the lowest Akaike Information Criterion (AIC) value was
111 selected as best fit from a nested series of potential models⁴⁴. Finally, we supplemented
112 4,967 modeled annual average concentrations in our database, accounting for about 6.3%
113 of the entire concentration dataset.

114 Moreover, we compared modeled with observed annual average concentrations and
115 fluxes (Supplementary Fig. 10) for 15,702 data points. Whereas the modeled
116 concentrations were on average 21% lower than the observed concentrations
117 (Supplementary Fig. 10a), the modeled and observed fluxes were similar with a
118 regression slope of 0.97 ($R^2 = 0.96$). This confirmed that the modeling approach was
119 able to estimate annual fluxes of dissolved solids in close agreement with direct
120 measurements, demonstrating the validity of our hybrid approach.

121 3.3 Global fluxes to the oceans

122 After determining the annual fluxes of DS for all the river stations, we calculated the
123 global fluxes of dissolved solids to the oceans using COSCAT (COastal Segmentation
124 and its related CATchment)⁴⁵ which is a well-established tool for estimating nitrogen
125 yield⁴⁵, natural riverine silica inputs⁴⁶ and river discharge^{45, 47} to the oceans. Here, we
126 applied the COSCAT methodology to estimate the fluxes of TDS and major ions (Ca²⁺,
127 Mg²⁺, Na⁺, K⁺, SO₄²⁻, Cl⁻, HCO₃⁻ and DSi) to coastal zones based on our dataset of
128 calculated fluxes with missing information taken from ancillary multi-averaged ion
129 concentrations provided by Meybeck and Ragu⁴⁸. For each COSCAT⁴⁷, the fluxes to
130 the oceans were calculated as follows:

131 For areas where data were available in our database, we computed the average yield
132 Y_j (Mt/(km²-yr)) in each COSCAT catchment ($j = 1$ to 151) from

$$133 Y_j = \frac{\sum_{i=1}^n \frac{F_{\text{basin } ij}}{A_{\text{basin } ij}}}{n_j} \quad (\text{S2})$$

134 and the fluxes in each COSCAT, $F_{\text{COSCAT } j}$ (Mt/yr) from

$$135 F_{\text{COSCAT } j} = Y_j \times A_{\text{COSCAT } j} \quad (\text{S3})$$

136 where $F_{\text{basin } ij}$ is an individual flux in the i -th sub-basin of the j -th COSCAT catchment
137 for stations in our database (Mt/yr), A_{basin} is the area of each sub-basin (km²), n is the
138 number of sub-basins, and $A_{\text{COSCAT } j}$ is the area of each COSCAT (km²) taken from
139 Meybeck et al.⁴⁵.

140 For the remaining COSCATs where data were not available in our database and the
141 dataset in Meybeck and Ragu⁴⁸ was instead used, we calculated the discharge-weighted
142 ion concentration Ion_j (mg/L) from

143
$$\text{Ion } *_{j} = \frac{\sum_{i=1}^n (C_{ij} \times Q_{ij})}{\sum Q_j} \quad (\text{S4})$$

144 and F_{COSCAT_j} in each COSCAT (Mt/yr) from

145
$$F_{\text{COSCAT}_j} = k \times \text{Ion } *_{j} \times Q_{\text{COSCAT}_j} \quad (\text{S5})$$

146 where $k = 0.001$ is the conversion coefficient, C_{ij} and Q_{ij} are the concentrations (mg/L)
 147 and corresponding river discharge (km^3/yr) at the i -th station of the j -th COSCAT
 148 catchment using information from the dataset of Meybeck and Ragu⁴⁸, Q_{COSCAT} (km^3/yr)
 149 was extracted from Durr et al.⁴⁶, and n is the number of stations in each COSCAT area.

150 For areas without any documented data, we calculated the fluxes in each COSCAT
 151 according to the method proposed by Durr et al.⁴⁶. We first calculated the discharge-
 152 weighted ion concentrations $\text{Ion } **_{j}$ (mg/L) in adjacent documented areas (using either
 153 our database or the dataset in Meybeck and Ragu⁴⁸) with similar weathering conditions
 154 and catchment properties, from:

155
$$\text{Ion } **_{j} = \frac{\sum_{i=1}^n (C_{*ij} \times Q_{*ij})}{\sum Q_{*j}} \quad (\text{S6})$$

156 where C_{*ij} and Q_{*ij} are the concentrations and corresponding river discharge at the i -th
 157 station in the j -th COSCAT catchment. We then extrapolated the $\text{Ion } *$ and $\text{Ion } **$ to the
 158 undocumented COSCAT catchment⁴⁶ and the flux was calculated as:

159
$$F_{\text{COSCAT}_j} = k \times (\text{Ion } *_{j} \text{ or } \text{Ion } **_{j}) \times Q_{\text{COSCAT}_j} \quad (\text{S7})$$

160 Finally, the total global fluxes were calculated as the sum of the fluxes in 151
 161 catchments in all COSCAT exorheic areas.

162
$$\text{Flux} = \sum_{j=1}^{151} F_{\text{COSCAT}_j} \quad (\text{S8})$$

163 **4. Trend analysis**

164 We used non-parametric Mann-Kendall (MK) method^{49, 50} to perform trend analysis

165 of time series of duration ≥ 5 years. In addition, trend-free pre-whitening (TFPW) in
 166 the R package ‘modifiedmk’ ensured data independence before implementing the MK
 167 test⁵¹. The overall procedure is called TFPW-MK (Trend-Free Pre-Whitening Mann-
 168 Kendall).

169 The MK statistic parameter (S) is determined from

$$170 \quad S = \sum_{k=1}^{n-1} \sum_{j=k+1}^n \text{sgn}(x_j - x_k) \quad (\text{S9})$$

171 in which

$$172 \quad \text{sgn}(x_j - x_k) = \begin{cases} 1, & x_j - x_k > 0 \\ 0, & x_j - x_k = 0 \\ -1, & x_j - x_k < 0 \end{cases} \quad (\text{S10})$$

173 where n is the number of data points in the time series, x_j and x_k are the j -th and k -th
 174 values in the new ordered data series obtained after eliminating the autocorrelation of
 175 the original data ($j > k$). For $n \geq 10$, the variance of S is obtained, using the normal
 176 approximation test, from

$$177 \quad \text{Var}(S) = \frac{[n(n-1)(2n+5) - \sum_{p=1}^q t_p(t_p-1)(2t_p+5)]}{18} \quad (\text{S11})$$

178 where q is the number of tied groups (or groups with the same value), and t_p is the
 179 number of samples in the p -th tied group. The Z parameter of the statistical test is:

$$180 \quad Z = \begin{cases} \frac{S-1}{\sqrt{\text{Var}(S)}}, & S > 0 \\ 0, & S = 0 \\ \frac{S+1}{\sqrt{\text{Var}(S)}}, & S < 0 \end{cases} \quad (\text{S12})$$

181 The time series exhibit an increasing trend with a positive Z value, and a decreasing
 182 trend with a negative Z value. The null hypothesis (H_0), which indicates no trend, is
 183 true if $-Z_{1-\alpha/2} \leq Z \leq Z_{1-\alpha/2}$ for a two-tailed test, in which α is the significance level.
 184 For $n \leq 10$, if S is positive (or negative) and the probability value according to n and S

185 (or absolute S) is less than $\alpha/2$ for a two-tailed test, then H_0 is rejected, and the trend is
186 either increasing or decreasing. In this study, a confidence level of 95% ($\alpha = 0.05$) was
187 used. $Z_{1-\alpha/2}$ is the critical value of Z from the standard normal table; for the 5%
188 significant level the value of $Z_{1-\alpha/2}$ is 1.96.

189 **5. Method for determining solute-induced river syndromes**

190 Based on the sum of total cation concentrations (Σ^+ , meq/L), Meybeck⁵² proposed
191 that ‘extremely dilute’ rivers with the least mineralized water have $\Sigma^+ < 0.185$ meq/L,
192 ‘dilute’ rivers have $\Sigma^+ < 0.75$ meq/L, ‘medium dilute’ rivers have $\Sigma^+ < 1.5$ meq/L,
193 ‘medium mineralized’ rivers have $1.5 \text{ meq/L} < \Sigma^+ < 3 \text{ meq/L}$, ‘mineralized’ rivers have
194 $\Sigma^+ > 3$ meq/L, and ‘saline’ rivers with the most mineralized water have $\Sigma^+ > 24$ meq/L.
195 In combination with the trend analysis, we further defined three solute-induced river
196 syndromes: salinization with $\Sigma^+ > 24$ meq/L and an increasing trend; mineralization
197 with $\Sigma^+ > 3$ meq/L and an increasing trend; and desalinization with $\Sigma^+ < 1.5$ meq/L and
198 a decreasing trend.

199 To determine whether a river experiences acidification or alkalization, both pH and
200 alkalinity (or acidity) must be considered^{4, 6, 53}. We calculated the ratio of hardness to
201 alkalinity, and extracted mean pH values for rivers from the GEMS (Global
202 Environment Monitoring System for Water) database⁵⁴. When the ratio of hardness to
203 alkalinity > 1 , acid input from anthropogenic sources is likely to be responsible³⁸. We
204 therefore propose the following diagnosis procedure. If the water $\text{pH} < 7$ and the ratio
205 of hardness to alkalinity > 1 and increasing with time in a river, the river is experiencing
206 an acidification syndrome. If $\text{pH} > 7$ and the ratio of hardness to alkalinity < 1 and

207 decreasing with time, the river is undergoing an alkalization syndrome.

208 Finally, we examined hardness (expressed as calcium carbonate equivalent in mg/L,
209 CaCO₃ mg/L) following the WHO classification of water hardness into soft (< 60 mg/L),
210 moderately hard (60-120 mg/L), hard (120-180 mg/L) and very hard (>180 mg/L)⁵⁵
211 levels. Thus, if river water has hardness > 120 mg/L with an increasing trend, the river
212 has a hardening syndrome. Conversely, if river water has hardness < 60 mg/L with a
213 decreasing trend, it has a softening syndrome.

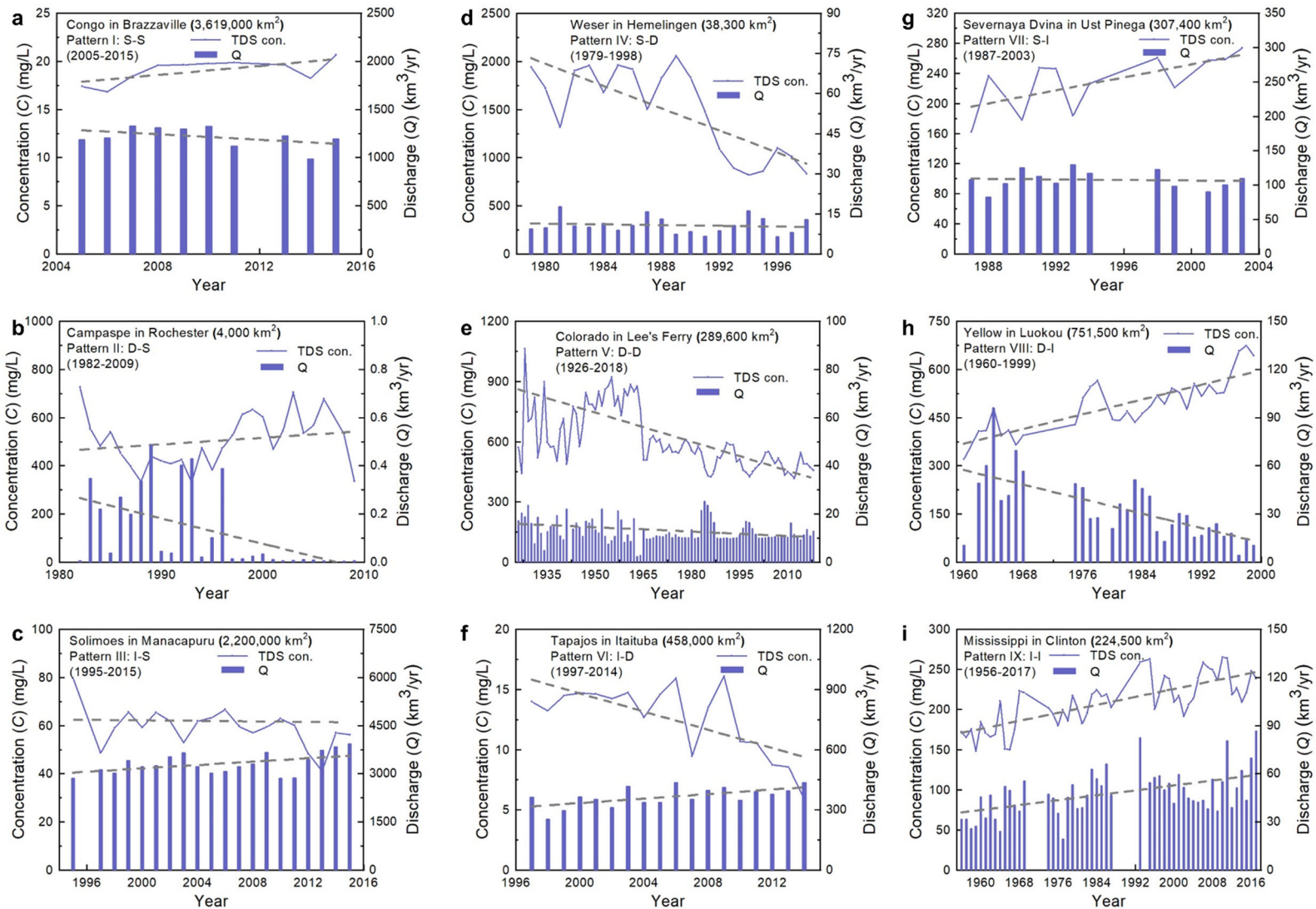
214 **6. Environmental factors extraction and latitudinal distribution**

215 First, the sub-basin boundaries were prepared for gauge stations. Catchment
216 boundaries were adopted from GSIM (The Global Streamflow Indices and Metadata
217 Archive)⁵⁶ according to the station coordinates for most sites. Following the catchment
218 delineation procedure⁵⁷, missing catchment boundaries were supplemented using
219 information from our datasets for other sites. We then used ArcGIS Map to extract
220 specific environmental factors.

221 The availability of catchment boundaries for each station enables association of
222 environmental variables to each gauge by extracting them from corresponding global-
223 scale gridded products. As summarized in Supplementary Table 6, 600 gauges of
224 catchment-scale metadata were derived from six global data products chosen to
225 represent natural and anthropogenic categories of catchment characteristics, with
226 lithology⁵⁸ and Köppen–Geiger climate^{59, 60} taken as natural factors. Land cover,
227 irrigation, dam, and population were considered as anthropogenic environmental
228 factors.

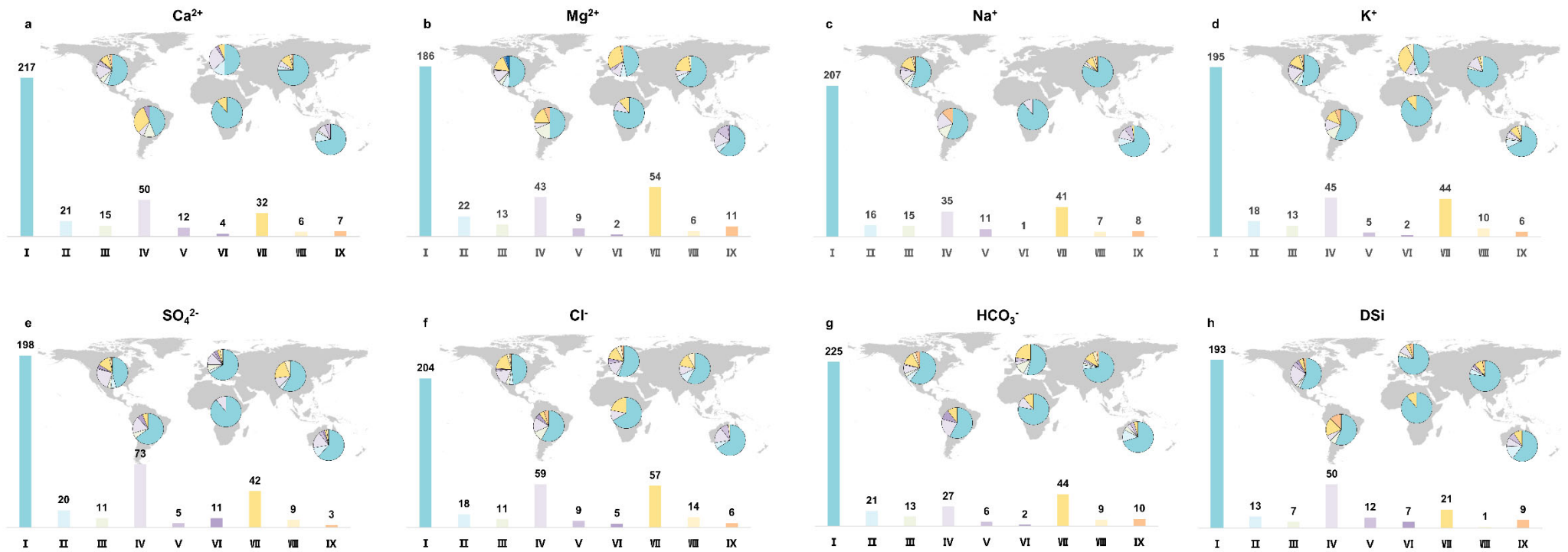
229 For lithology in GLiM (Global Lithological Map), we reclassified the original 15
230 lithological subclasses and obtained four new lithological sub-classes (sedimentary,
231 volcanic (igneous) rocks, metamorphic rocks, and ice). The Köppen–Geiger climate
232 classification system, which comprised 31 climate classes each described by a three-
233 letter code, was reclassified into arid, temperate, tropical, cold, and polar types. In the
234 same way, GLCNMO (Global Land Cover by National Mapping Organization)⁶¹ was
235 reclassified into vegetation, urban, agriculture, and bare land. Moreover, we selected
236 irrigation as a percentage of total grid cell area⁶², DOR (degree of regulation) from
237 GRanD (Global Reservoir and Dam Database)⁶³ and discharge in our datasets related
238 to dams, and population density from GPWv4 (Gridded Population of the World version
239 4)⁶⁴ as representative quantitative anthropogenic factors. We then plotted the latitudinal
240 distribution of typical environmental factors (carbonate sedimentary rocks, acid
241 volcanic rock, arid climate classification, temperate climate classification, global
242 irrigation area, and urban land cover classification) as the percentage ratio of the
243 specific factor area at a given latitude to its worldwide area in Fig. 5c and d, and
244 Supplementary Fig. 7.

245 Finally, we extracted sub-classified factors of each global product for all available
246 catchments using ArcGIS Map. Then we summarized the proportional information on
247 the various environmental factors for 600 river stations. These metadata (comprising
248 percentages of different classes of catchment characteristics, and representing the
249 characteristics of the upstream catchment for each streamflow gauge) were calculated
250 from the gridded data masked.

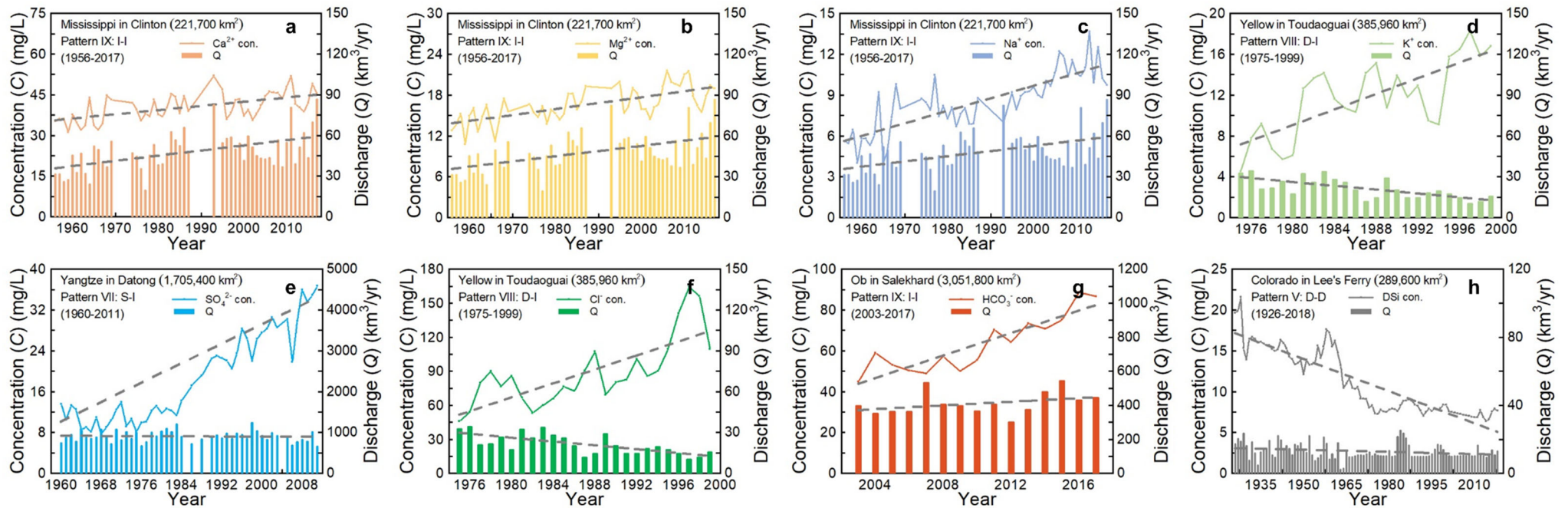


251
 252 **Supplementary Fig. 1 Representative large rivers for nine $[Q, C]$ co-patterns showing discharge (Q , histograms), total dissolved**

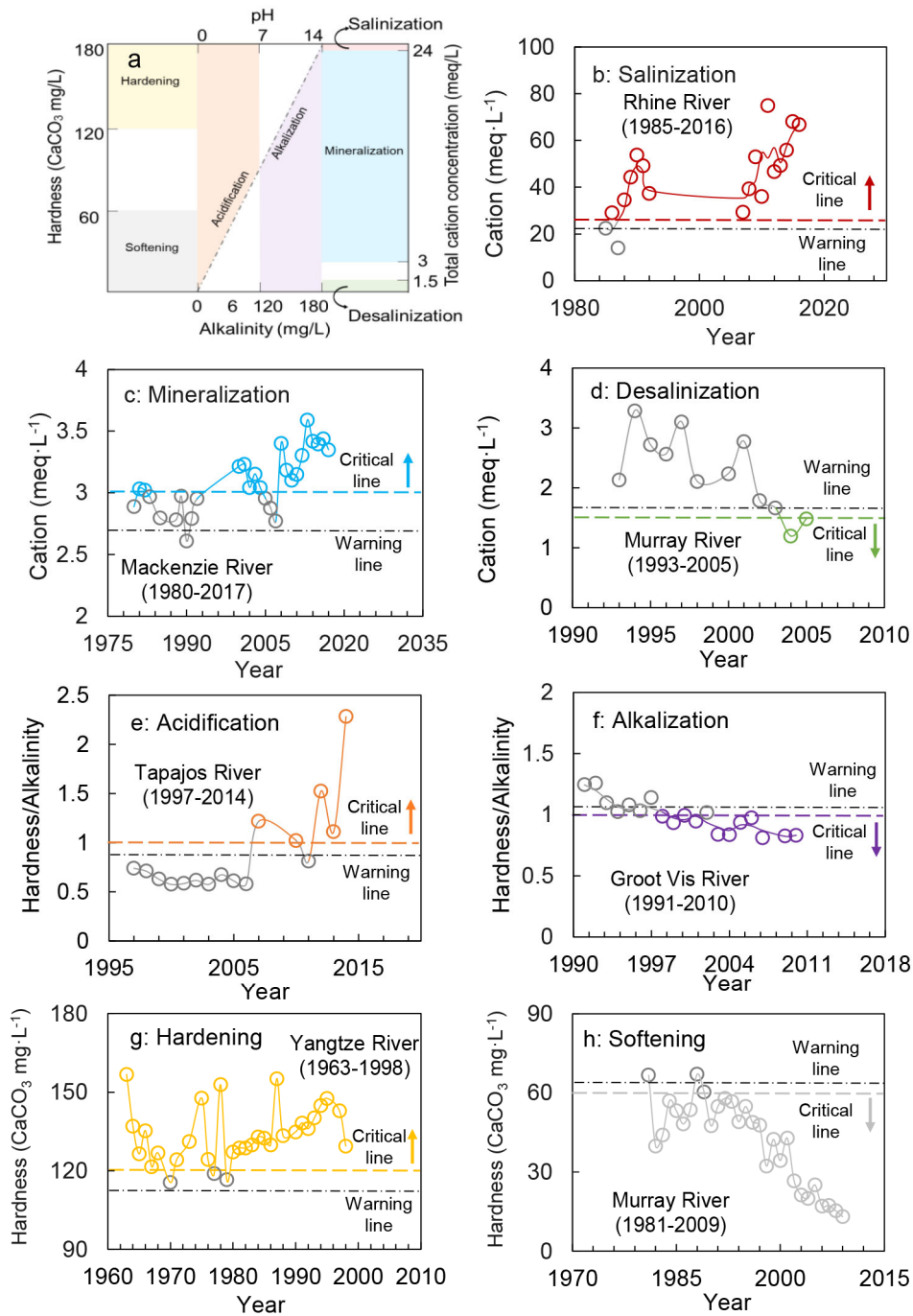
253 **solids (TDS) concentrations (C, solid line), and corresponding trends (grey dashed lines).** In the nine patterns, S represents stable
254 trend, I represents increasing trend, and D represents decreasing trend. **(a)** Congo River at Brazzaville, **(b)** Campaspe River at Rochester,
255 **(c)** Solimoes River at Manacapuru, **(d)** Weser River at Hemelingen, **(e)** Colorado River at Lee's Ferry, **(f)** Tapajós River at Itaituba, **(g)**
256 Severnaya Dvina River at Ust Pinega, **(h)** Yellow River at Luokou, and **(i)** Mississippi River at Clinton. All trends are significant at the
257 0.05 significance level, and the dashed lines are the regression lines.



259 **Supplementary Fig. 2** Nine [Q , C] co-varying patterns for discharge (Q) and dissolved solids concentrations (C), and their global
 260 **distributions.** a~h represent Ca²⁺, Mg²⁺, Na⁺, K⁺, SO₄²⁻, Cl⁻, HCO₃⁻, and dissolved silica (DSi). Histograms show the distribution of nine
 261 patterns in each continent and the number of river stations exhibiting each pattern in the world's large rivers. All trends are significant at
 262 the 0.05 significance level.



264 **Supplementary Fig. 3** Representative large rivers for nine [Q , C] co-varying patterns showing discharge (Q , histograms), dissolved
 265 ion concentrations (C , solid line), and corresponding trends (grey dashed lines). In the nine patterns, S represents stable trend, I
 266 represents increasing trend, and D represents decreasing trend. (a) Ca^{2+} : Clinton at Mississippi River, (b) Mg^{2+} : Clinton at Mississippi
 267 River, (c) Na^{+} : Clinton at Mississippi River, (d) K^{+} : Toudaoguai at Yellow River, (e) SO_4^{2-} : Datong at Yangtze River, (f) Cl^{-} : Toudaoguai
 268 at Yellow River, (g) HCO_3^{-} : Salekhard at Ob' River, (h) dissolved silica (DSi): Lee's Ferry at Colorado River. All trends are significant at
 269 the 0.05 significance level.



270

271 **Supplementary Fig. 4 Warning signs and thresholds of solute metrics for**

272 **identification of solute-induced river syndromes. a** illustrates the thresholds of solute

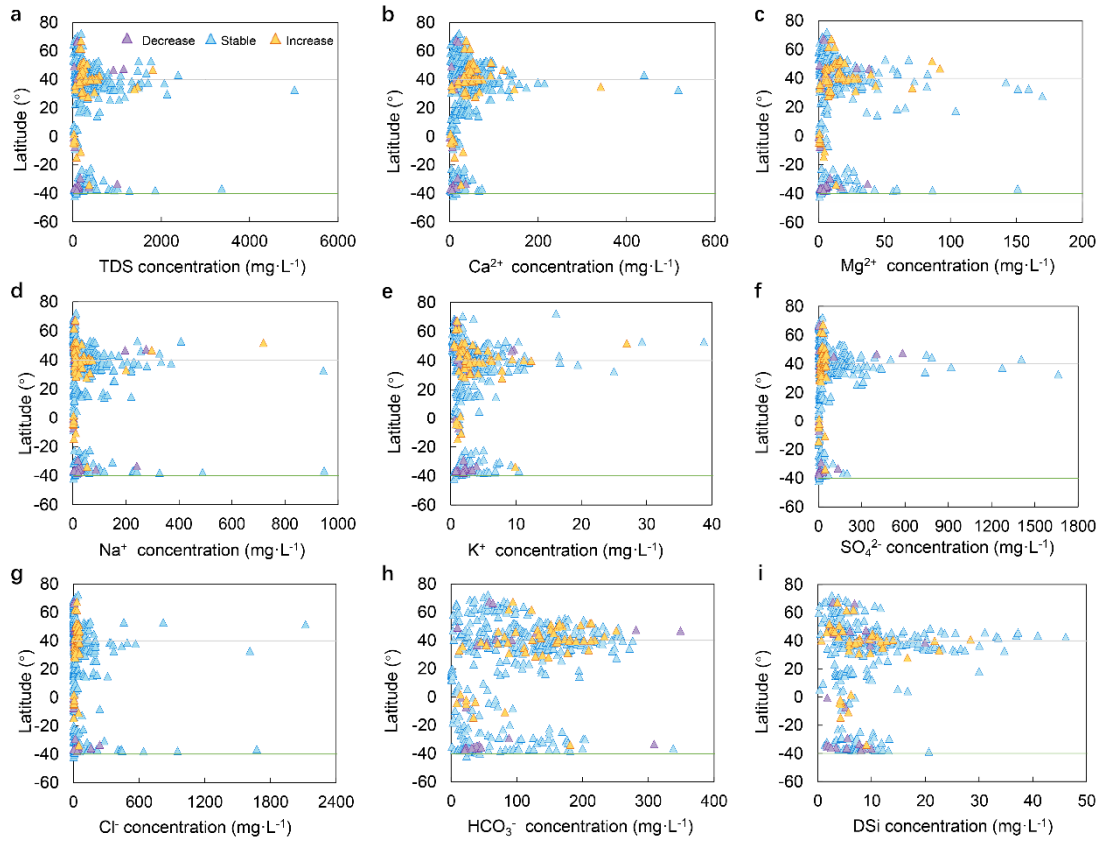
273 metrics used to identify solute-induced river syndromes. **b-h** present seven river

274 syndromes associated with temporal variation in solute concentration. The critical line

275 indicates the threshold used to identify a solute-induced river syndrome. The warning

276 line represents the status when a specific solute metric reaches 90% of one of the

277 corresponding thresholds (e.g. Σ^+ ($\text{Ca}^{2+}+\text{Mg}^{2+}+\text{Na}^++\text{K}^+$) at 21.6 meq/L, 2.7 meq/L, and
278 1.7 meq/L for salinization, mineralization, and desalinization; hardness/alkalinity at 0.9
279 and 1.1 for acidification and alkalization; and hardness (CaCO_3) at 108 mg/L and 66
280 mg/L for hardening and softening).



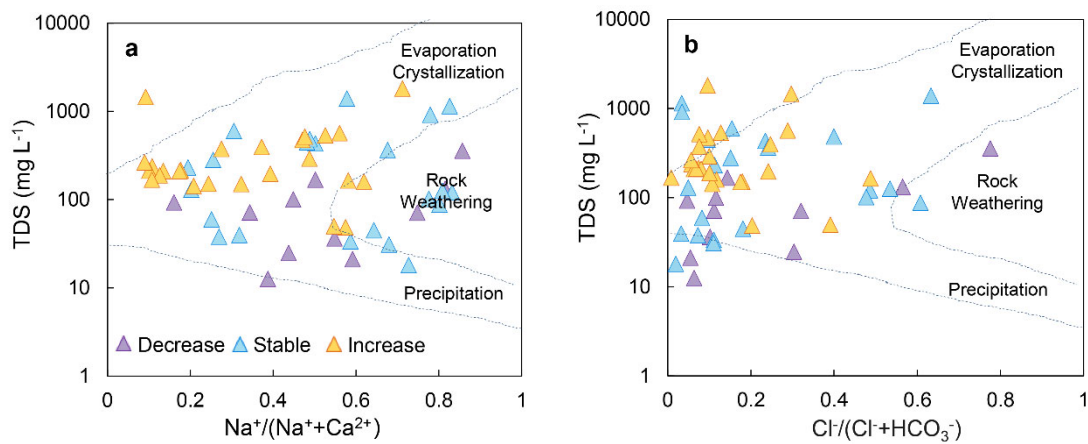
281

282 **Supplementary Fig. 5 Latitudinal distribution of mean annual solute**

283 **concentrations. a, Total dissolved solids (TDS). b, Ca²⁺. c, Mg²⁺. d, Na⁺. e, K⁺. f, SO₄²⁻.**

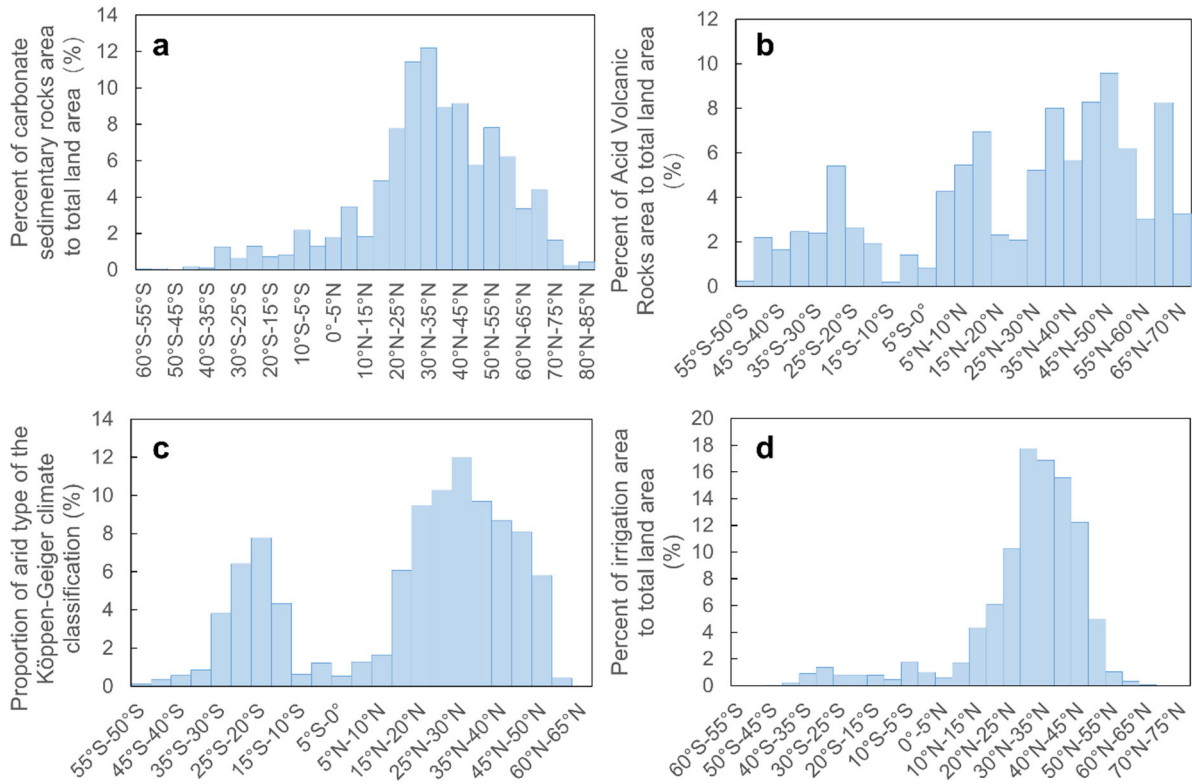
284 **g, Cl⁻. h, HCO₃⁻. i, Dissolved silica (DSi). Purple, blue, and yellow triangles**

285 **respectively represent rivers with decreasing, stable, and increasing trends in solutes.**



286

287 **Supplementary Fig. 6 Gibbs model for stations with solute-induced river**
 288 **syndromes with varying trends in total dissolved solids (TDS) concentrations in**
 289 **three typical latitudinal belts. Purple, blue, and yellow triangles respectively**
 290 **represent gauge stations with decreasing, stable, and increasing TDS trends.**



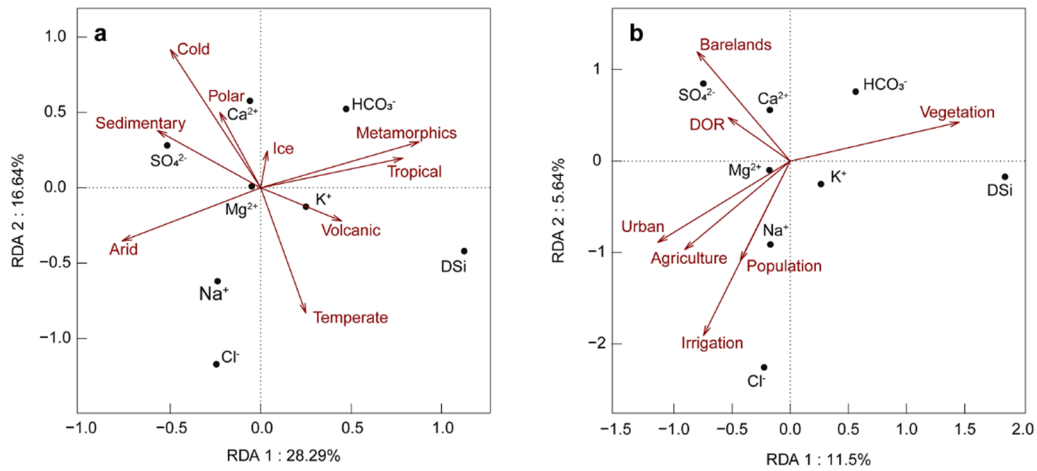
291

292 **Supplementary Fig. 7 Latitudinal distribution of typical environmental factors.**

293 **a~d** show latitudinal distributions of carbonate sedimentary rock, acid volcanic

294 (igneous) rocks, arid climate classification, and irrigation area.

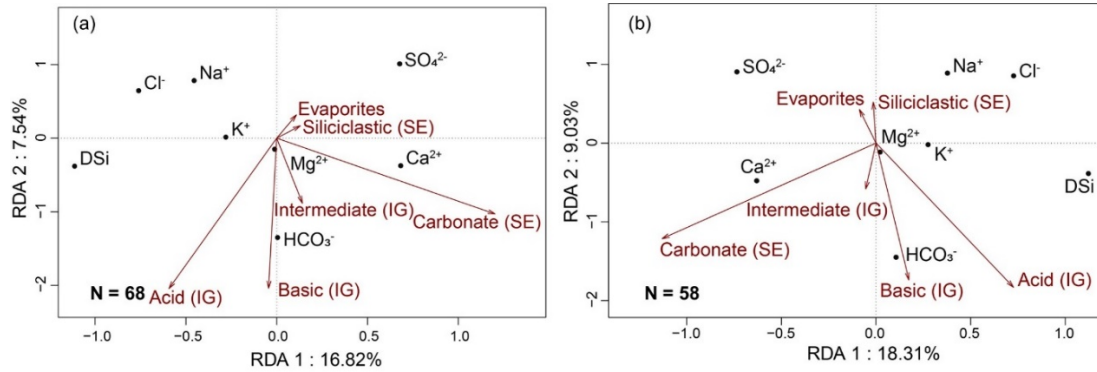
295



296

297 **Supplementary Fig. 8 Redundancy analysis (RDA) results for dissolved solids and**
298 **environmental factors in the world's large rivers. a, for natural factors**
299 **(reclassification for Köppen climate and lithology) in 68 sites with solute-induced river**
300 **syndromes. b, for anthropogenic factors (irrigation, population, degree of regulation**
301 **(DOR), and detailed reclassification of land cover) in 68 sites with solute-induced river**
302 **syndromes. DSi represents dissolved silica.**

303



304

305 **Supplementary Fig. 9 Redundancy analysis (RDA) for dissolved solids in the**

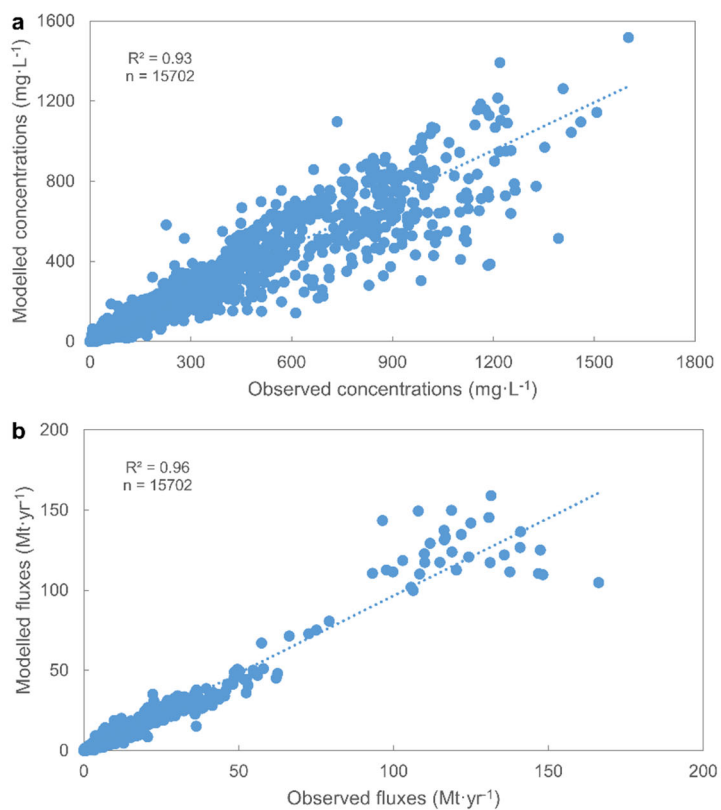
306 **world's large rivers for natural factors (sub-classification of sedimentary and**

307 **igneous (volcanic) rocks). a, in 68 sites with solute-induced river syndromes. b, in 58**

308 **sites with solute-induced river syndromes in critical latitudinal belts. IG and SE**

309 **represent igneous and sedimentary rocks. DSi represents dissolved silica.**

310



311

312 **Supplementary Fig. 10 Comparison between observed and modeled dissolved solid**
313 **concentrations (a) and fluxes (b), and linear regressions (dashed lines).**

314

315 **Supplementary Table 1** Summary of underlying natural and human causes of water quality in total dissolved solids (TDS) trends for
 316 nine [Q , C_{TDS}] co-varying patterns of discharge (Q) and TDS concentrations (C_{TDS})

Pattern	Representative gauge station in world's large river	Causes for [Q , C_{TDS}] trends
Pattern I	Congo River at Brazzaville	The Brazzaville station in the Congo River of Africa had relatively stable Q and C_{TDS} (Pattern I) from 2005-2015, as shown in Supplementary Fig. 1a. This is reasonable because the river is located in a geologically old and highly degraded shield, and its basin comprises 50% tropical rain forest and has experienced negligible changes in precipitation over several decades ^{65, 66} .
Pattern II	Campaspe River at Rochester	The large decrease of annual discharge in the Campaspe River (Supplementary Fig. 1b), affecting the whole of southern Australia ⁶⁷ , likely resulted from lower autumn and winter rainfall, fewer high rainfall years, and increased temperature ⁶⁸ . However, effective salinity control in the Rochester Irrigation Area has helped maintain stable C_{TDS} over time ⁶⁹ .
Pattern III	Solimoes River at Manacapuru	The Solimoes River, the largest tributary of the Amazon River, experienced stable TDS and increasing river discharge between 1995-2015 at the Manacapuru station (Pattern III, Supplementary Fig. 1c). This was due to increasing atmospheric water vapor import from the warming tropical Atlantic and intensified chemical weathering by higher precipitation, which compensated C_{TDS} dilution by the increased river discharge ⁷⁰ .
Pattern IV	Weser River at Hemelingen	The Weser River had a sharp decline of TDS and a stable river discharge trend between 1979 and 1998 (Pattern IV, Supplementary Fig. 1d), due to reduced human interference (e.g., mining, agriculture, etc.) and effective conservation management ^{71, 72} .
Pattern V	Colorado River at Lee's Ferry	The Colorado River at Lee's Ferry station exhibited decreasing Q and C_{TDS} between 1926 and 2018 (Pattern V, Supplementary Fig. 1e), which could be attributed to damming and conservation management for decreasing TDS ⁷³ , severe climate change ⁷⁴ , droughts ⁷⁵ and increasing water withdrawal in the upper Colorado River Basin from 1995 to 2000 for decreasing river discharge ⁷⁶ .

317

318 **Supplementary Table 1** Summary of underlying natural and human causes of water quality in total dissolved solids (TDS) trends for
 319 nine [Q , C_{TDS}] co-varying patterns of discharge (Q) and TDS concentrations (C_{TDS}) (*continued*)

Pattern	Representative gauge station in world's large river	Causes for [Q , C_{TDS}] trends
Pattern VI	Tapajós River at Itaituba	The Tapajós River, the fifth largest tributary of the Amazon River in the central north of Brazil ⁷⁷ , experienced decreasing C_{TDS} and increasing river discharge (Pattern VI, Supplementary Fig. 1f) between 1997 and 2014. Compared with the Amazonian Solimoes River, the discharge of the Tapajós River was ten times lower because of its smaller basin size. Limited TDS loading, river dilution ⁷⁸ and basin effects ⁷⁰ could have contributed to the decreasing trend in TDS concentration.
Pattern VII	Severnaya Dvina River at Ust Pinega	In the Arctic region, the Severnaya Dvina (S. Dvina) River at Ust Pinega station (Pattern VII, Supplementary Fig. 1g) exhibited no river discharge trend variations resulting from longer ice duration ^{79, 80} . The significant increase in TDS concentration was probably due to accelerated elemental cycling and export through increased plant productivity in a warming climate ^{81, 82} .
Pattern VIII	Yellow River at Luokou	The discharge at the Luokou station in the lower reach of the Yellow River displayed a sharp decreasing trend, caused by decreasing precipitation, and increasing water withdrawal for intensified agricultural irrigation ⁸³ , whereas the increasing C_{TDS} trend is mainly attributed to the concentration effect of low river flow ⁶⁵ and saline irrigation return waters ⁷ (Pattern VIII, Supplementary Fig. 1h).
Pattern IX	Mississippi River at Clinton	At Clinton Station, the Mississippi River showed increasing Q and C_{TDS} between 1956-2017 (Supplementary Fig. 1i, in agreement with Raymond et al. ⁸⁴ who reported increasing river discharge and HCO_3^- concentrations, mainly due to agricultural practices (e.g., fertilizer use, liming, and irrigation). The present study corroborates earlier findings that continental US rivers have been experiencing freshwater salinization syndrome ⁸⁵ .

320

321 **Supplementary Table 2** Estimated global fluxes of dissolved solids to the oceans

Discharge km ³ /yr	Year	Area Mkm ²	TDS	Ca ²⁺	Mg ²⁺	Na ⁺	K ⁺ Mt/yr	SO ₄ ²⁻	Cl ⁻	HCO ₃ ⁻	DSi	References
31400	1989	/	3600	500	124.8	138	46.8	294	117.15	1989	390	⁸⁶
37400	1999	148.17	3618	500	126	195	48	202	217	1946	389	⁸⁷
36000	2011	105	3800	/	/	/	/	/	360	/	330	⁷¹
39080	2019	114.7	6393	783	215	362	78	711	652	2421	363	Present study

322 Note: TDS represents total dissolved solids; DSi represents dissolved silica.

323 **Supplementary Table 3** Summary of redundancy analysis (RDA) vector reports for dissolved solids concentrations and typical natural
 324 environmental factors at 68 sites with solute-induced river syndromes and 58 syndrome sites in the critical latitudinal belts (“***”, “**”,
 325 “*”, “.”, and “ ” represent correlations at significant levels of 0.001, 0.01, 0.05, 0.1, and 1 (2-tailed); r^2 indicates correlation coefficient
 326 square; α indicates significance. The symbols have the same meanings in the following tables)

Environmental factors	68 sites					58 sites				
	R1	R2	r^2	p	α	R1	R2	r^2	p	α
Tropical	0.98	0.20	0.23	0.001	***	-0.98	-0.18	0.25	0.001	***
Arid	-0.93	-0.37	0.25	0.001	***	0.93	0.36	0.26	0.001	***
Temperate	0.34	-0.94	0.28	0.001	***	-0.47	0.88	0.27	0.001	***
Cold	-0.53	0.85	0.41	0.001	***	0.61	-0.79	0.43	0.001	***
Polar	-0.46	0.89	0.11	0.024	*	0.51	-0.86	0.13	0.022	*
Sedimentary	-0.85	0.53	0.18	0.001	***	0.91	-0.42	0.17	0.01	**
Volcanic	0.90	-0.43	0.09	0.032	*	-0.90	0.43	0.12	0.038	*
Metamorphic	0.96	0.28	0.30	0.001	***	-0.94	-0.33	0.33	0.001	***
Ice	0.12	0.99	0.02	0.367		0.97	0.26	0.01	0.817	

327

328

329 **Supplementary Table 4** Summary of redundancy analysis (RDA) vector reports for dissolved solids concentrations and typical
 330 anthropogenic environmental factors at 68 sites with solute-induced river syndromes and 58 syndrome sites in the critical latitudinal belts

Environmental factors	68 sites					58 sites				
	R1	R2	r ²	p	α	R1	R2	r ²	p	α
Population	-0.57	-0.82	0.04	0.300		0.95	0.32	0.03	0.508	
Vegetation	1.00	0.09	0.13	0.012	*	-1.00	0.03	0.14	0.016	*
Agriculture	-0.89	-0.46	0.07	0.086	.	1.00	-0.03	0.09	0.066	.
Bare land	-0.79	0.62	0.08	0.064	.	0.87	-0.50	0.11	0.052	.
Urban	-0.94	-0.33	0.09	0.042	*	1.00	0.05	0.10	0.072	.
Irrigation	-0.57	-0.82	0.12	0.028	*	0.76	0.64	0.13	0.019	*
DOR	-0.89	0.45	0.03	0.439		0.71	-0.71	0.06	0.193	

331 Note: DOR represents degree of regulation.

332

333 **Supplementary Table 5** Summary of redundancy analysis (RDA) vector reports for dissolved solids concentrations and sub-classified
 334 rocks at 68 sites with solute-induced river syndromes and 58 syndrome sites in the critical latitudinal belts

Environmental factors	68 sites					58 sites				
	R1	R2	r ²	<i>p</i>	α	R1	R2	r ²	<i>p</i>	α
Acid (IG)	-0.78	-0.62	0.19	0.001	***	0.87	-0.49	0.23	0.002	**
Basic (IG)	0.08	-1.00	0.12	0.019	*	0.17	-0.99	0.10	0.050	*
Intermediate (IG)	0.64	-0.77	0.03	0.336		-0.52	-0.86	0.01	0.686	
Evaporites	0.84	0.54	0.01	0.860		0.14	0.99	0.01	0.868	
Siliciclastic (SE)	0.98	0.21	0.01	0.844		-0.56	0.83	0.01	0.816	
Carbonate (SE)	0.96	-0.26	0.47	0.001	***	-0.94	-0.35	0.51	0.001	***

335 Note: IG and SE represent igneous (volcanic) and sedimentary rocks, respectively.

336

337 **Supplementary Table 6** Global data products used for extracting natural and anthropogenic factors driving water chemistry in the world's
 338 large rivers

Variables	Data sources	Spatial resolution	Reference period
	The Global Lithological Map v1.0 (GLiM) dataset (Hartmann and Moosdorf, 2012 ⁵⁸)		
Lithology	https://www.clisap.de/research/b:-climate-manifestations-and-impacts/crg-chemistry-of-natural-aqueous-solutions/global-lithological-map/ (last access: 15 Dec. 2019)	0.5 arc deg × 0.5 arc deg	--
Climate type	World map of Köppen–Geiger climate classification system (Rubel and Kottek, 2010 ⁵⁹) http://koeppen-geiger.vu-wien.ac.at (last access: 15 Dec. 2019)	5 arcmin × 5 arcmin	1951-2000
Land cover	Global Land Cover by National Mapping Organizations (GLCNMO) (Tateishi et al., 2011 ⁶¹) http://www.iscgm.org/ (last access: 15 Dec. 2019)	30 arcsec × 30 arcsec	2003
Irrigation	Global Map of Irrigation Areas version 5 (Siebert et al., 2019 ⁶²) http://www.fao.org/aquastat/en/geospatial-information/global-maps-irrigated-areas/latest-version (last access: 15 Dec. 2019)	5 arcmin × 5 arcmin	Around 2005
Dams	Global Reservoir and Dam (GRanD), version 1 (Lehner et al., 2011 ⁶³) http://sedac.ciesin.columbia.edu/data/set/grand-v1-dams-rev01 (last access: 15 Dec. 2019)	6862 data points storage capacity of more than 0.1 km ³	--
Population	Gridded Population of the World (GPW) version 4 (CIESIN, 2016 ⁶⁴) http://sedac.ciesin.columbia.edu/data/set/gpw-v4-population-count (last access: 15 Dec. 2019)	30 arcsec × 30 arcsec	2005

339

340 **Supplementary Table 7** Data sources for concentrations of dissolved ions in world's large rivers

Data sources	Number of sites	Record years	Access time
Arctic Great Rivers Observatory (ARCTIC-GRO)	6	2003-2017	Sep. 2018
Australian databases (Provincial Survey of New South Wales, Waterwatch Victoria, and Environmental Protection Agency for South Australia)	64	1973-2008	Sep. 2019
Canada's National Water Data Archive (HYDAT)	37	1970-2017	Sep. 2018
Confederación Hidrográfica del Ebro	1	1987-2014	Sep. 2018
Datenportal der Flussgebietsgemeinschaft (FGG) Elbe	1	1980-2016	Sep. 2018
Flussgebietsgemeinschaft Weser (FGG Weser)	2	1979-2016	Sep. 2018
Global Environment Monitoring System for Water (GEMS)	312	1966-2016	Sep. 2018
Hydrological Yearbooks of the People's Republic of China	5	1964-2011	Sep. 2018
Rijkswaterstaat	4	1960-2016	Sep. 2018
the Observation Service SO HYBAM (HYBAM)	18	1994-2016	Sep. 2018
United States Geological Survey (USGS)	190	1915-2018	Sep. 2019
Literature sources	29	1958-2012	Sep. 2018

341

342

343 **Supplementary Table 8** Data sources for runoff in world's large rivers

Data sources	Number of sites	Record years	Access time
Arctic Great Rivers Observatory (ARCTIC-GRO)	6	2003-2017	Sep. 2018
Australian databases (Provincial Survey of New South Wales, Waterwatch Victoria, and Environmental Protection Agency for South Australia)	58	1973-2011	Sep. 2019
Canada's National Water Data Archive (HYDAT)	36	1970-2016	Sep. 2018
Confederación Hidrográfica del Ebro	1	1987-2014	Sep. 2018
Datenportal der Flussgebietsgemeinschaft (FGG) Elbe	1	1980-2016	Sep. 2018
Equipe d'Administration de la Banque HYDRO (HYDRO)	2	1979-1993	Sep. 2018
Flussgebietsgemeinschaft Weser (FGG Weser)	2	1979-2015	Sep. 2018
PKU-IEE- WLRs-WS-NL2006 Database	417	1946-2018	Sep. 2019
Rijkswaterstaat	4	1961-2016	Sep. 2018
The Observation Service SO HYBAM (HYBAM)	18	1994-2016	Sep. 2018
United States Geological Survey (USGS)	127	1951-2018	Sep. 2019
Literature and online web sources	29	1960-2015	Sep. 2018

344

345 **Supplementary Table 9** Numbers of stations with dissolved solids concentration (DS,
 346 C) and river runoff (*Q*) data of various record lengths

Record length (Years)	Ca ²⁺	Mg ²⁺	Na ⁺	K ⁺	SO ₄ ²⁻	Cl ⁻	HCO ₃ ⁻	DSi ^b	TDS ^c	<i>Q</i>
<5	65	63	78	75	72	75	82	52	91	104
[5, 10) ^a	62	50	63	66	66	76	67	64	89	83
[10, 20)	147	132	139	130	141	149	152	114	131	151
[20, 30)	90	91	77	78	94	91	92	74	85	96
[30, 40)	40	41	38	38	41	47	41	37	42	43
[40, 50)	27	28	27	26	30	24	21	21	28	30
≥50	28	26	25	25	31	36	18	23	29	39
Sum	459	431	447	438	475	498	473	385	495	546

347 ^a Right parenthesis indicates that record length is not inclusive.

348 ^b Dissolved silica.

349 ^c Total dissolved solids.

350

351 **Supplementary References**

- 352 1. Chapman, D. V., World Health Organization. Water quality assessments: a guide to
353 the use of biota, sediments and water in environmental monitoring (CRC Press,
354 Cambridge, 1996).
- 355 2. Li, S. Y. & Bush, R. T. Changing fluxes of carbon and other solutes from the
356 Mekong River. *Sci. Rep.* **5**, 1-16 (2015).
- 357 3. Müller, B., Berg, M., Pernet-Coudrier, B., Qi, W. & Liu, H. The geochemistry of
358 the Yangtze River: Seasonality of concentrations and temporal trends of chemical
359 loads. *Global Biogeochem. Cycles* **26**, 1-14 (2012).
- 360 4. Chen, J. S., Wang, F. Y., Xia, X. H. & Zhang, L. T. Major element chemistry of the
361 Changjiang (Yangtze River). *Chem. Geol.* **187**, 231-255 (2002).
- 362 5. Dai, Z. J., Du, J. Z., Zhang, X. L., Su, N. & Li, J. F. Variation of Riverine Material
363 Loads and Environmental Consequences on the Changjiang (Yangtze) Estuary in
364 Recent Decades (1955-2008). *Environ. Sci. Technol.* **45**, 223-227 (2011).
- 365 6. Chen, J. S., et al. Spatial and temporal analysis of water chemistry records (1958-
366 2000) in the Huanghe (Yellow River) basin. *Global Biogeochem. Cycles* **19**, 1-27
367 (2005).
- 368 7. Chen, J. S., He, D. W. & Cui, S. B. The response of river water quality and quantity
369 to the development of irrigated agriculture in the last 4 decades in the Yellow River
370 Basin, China. *Water Resour. Res.* **39**, 1-11 (2003).
- 371 8. Chen, J. S., Guan, W. R., Xia, X. H. & He, D. W. A probe into several problems of
372 water-quality trends in the mainstream of Yangtze River from 1960's to 1980's.

- 373 *Environmental Chemistry* **1**, 8-13 (1998). in Chinese.
- 374 9. Xie, C. J., Gao, Q. Z., Tao, Z., Liu, L. H. & Li, S. C. Chemical weathering and CO₂
375 consumption in the Dongjiang River Basin. *Acta Scientiae Circumstantiae* **8**, 2123-
376 2133 (2013). in Chinese.
- 377 10. Li, D. The study on the hydro-chemical characteristics and the flux to the sea about
378 the Rivers in the East of China (East China Normal University, Shanghai, 2009).
379 in Chinese.
- 380 11. Liu, X. C., Shen, H. T. & Huang, Q. H. Concentration variation and flux estimation
381 of dissolved inorganic nutrient from the Changjiang River into its estuary.
382 *Oceanologia et limnologia sinica* **3**, 332-340 (2002). in Chinese.
- 383 12. Shen, Z. L. A study on the effects of the Three Gorge Project on the distributions
384 and changes of the nutrients in the Changjiang River estuary. *Oceanologia et*
385 *limnologia sinica* **22**, 540-546 (1991). in Chinese.
- 386 13. Wang, J. C., Bian, J. J. & Chen, X. G. Analysis on changing tendency of water
387 quality in trunk stream of Yangtze River Since 2000. *HubeiWater Power* **2**, 1-3
388 (2009). in Chinese.
- 389 14. Xia, X. Q., et al. Major ion chemistry in the Yangtze River. *Earth Sci. Front.* **15**,
390 194-202 (2008). in Chinese.
- 391 15. Xia, X. J., Xu, J., Feng, W. J. & Li, Q. The relationship between discharge to the
392 sea and in Datong-Xuliujing of Yangtze River. *ZhongGuoShuiYun* **6**, 71-73 (2016).
393 in Chinese.
- 394 16. Biggs, T., et al. Closing of the Krishna Basin: Irrigation, streamflow depletion and

- 395 macroscale hydrology (International Water Management Institute, Colombo, 2007).
- 396 17. Bouraoui, F. & Grizzetti, B. Long term change of nutrient concentrations of rivers
397 discharging in European seas. *Sci. Total Environ.* **409**, 4899-4916 (2011).
- 398 18. Chetelat, B., et al. Geochemistry of the dissolved load of the Changjiang Basin
399 rivers: Anthropogenic impacts and chemical weathering. *Geochim. Cosmochim.*
400 *Acta* **72**, 4254-4277 (2008).
- 401 19. European Marine Observation and Data Network. Time series of annual water
402 discharge. [http://www.emodnet-](http://www.emodnet-arctic.eu/content/content.php?menu=19&htm=78#)
403 [arctic.eu/content/content.php?menu=19&htm=78#](http://www.emodnet-arctic.eu/content/content.php?menu=19&htm=78#) (2019).
- 404 20. Gao, Q. Z., et al. Chemical weathering and CO₂ consumption in the Xijiang River
405 basin, South China. *Geomorphology* **106**, 324-332 (2009).
- 406 21. Gong, Y., et al. Seasonal Variation and Sources of Dissolved Nutrients in the Yellow
407 River, China. *Int. J. Env. Res. Public Health* **12**, 9603-9622 (2015).
- 408 22. Jian, J., Webster, P. J. & Hoyos, C. D. Large-scale controls on Ganges and
409 Brahmaputra river discharge on intraseasonal and seasonal time-scales. *Q. J. R.*
410 *Meteorol. Soc.* **135**, 353-370 (2009).
- 411 23. Li, M. T., Xu, K. Q., Watanabe, M. & Chen, Z. Y. Long-term variations in dissolved
412 silicate, nitrogen, and phosphorus flux from the Yangtze River into the East China
413 Sea and impacts on estuarine ecosystem. *Estuar. Coast. Shelf Sci.* **71**, 3-12 (2007).
- 414 24. Li, S. Y., Lu, X. X. & Bush, R. T. Chemical weathering and CO₂ consumption in
415 the Lower Mekong River. *Sci. Total Environ.* **472**, 162-177 (2014).
- 416 25. Li, S. Y. & Bush, R. T. Rising flux of nutrients (C, N, P and Si) in the lower Mekong

- 417 River. *J. Hydrol.* **530**, 447-461 (2015).
- 418 26. Lu, X. X., Li, S. Y., Kummu, M., Padawangi, R. & Wang, J. J. Observed changes
419 in the water flow at Chiang Saen in the lower Mekong: Impacts of Chinese dams?
420 *Quat. Int.* **336**, 145-157 (2014).
- 421 27. Negrel, P., Roy, S., Petelet-Giraud, E., Millot, R. & Brenot, A. Long-term fluxes of
422 dissolved and suspended matter in the Ebro River Basin (Spain). *J. Hydrol.* **342**,
423 249-260 (2007).
- 424 28. Ollivier, P., Radakovitch, O. & Hamelin, B. Major and trace element partition and
425 fluxes in the Rhône River. *Chem. Geol.* **285**, 15-31 (2011).
- 426 29. OSPAR Commission. Technical supplement 4 - Complementary graphic
427 presentation of catchment data in 1990-2006: Assessment of riverine inputs and
428 direct discharges of nutrients and selected hazardous substances to OSPAR
429 maritime area in 1990-2006 (2019).
- 430 30. Ouyang, S., et al. Impact of Water Diversion of the South-to-North Water Diversion
431 Middle Route Project on the Hydrological Characteristics at the Junction of
432 Yangtze River and Poyang Lake (Destech Publications, Lancaster, 2016).
- 433 31. Ran, L. S., Lu, X. X., Sun, H. G., Han, J. T. & Yu, R. H. Chemical denudation in
434 the Yellow River and its geomorphological implications. *Geomorphology* **231**, 83-
435 93 (2015).
- 436 32. Singh, S. K., Sarin, M. M. & France L. C. Chemical erosion in the eastern Himalaya:
437 Major ion composition of the Brahmaputra and $\delta^{13}\text{C}$ of dissolved inorganic carbon.
438 *Geochim. Cosmochim. Acta* **69**, 3573-3588 (2005).

- 439 33. Sun, H. G., Han, J. T., Li, D., Zhang, S. R. & Lu, X. X. Chemical weathering
440 inferred from riverine water chemistry in the lower Xijiang basin, South China. *Sci.*
441 *Total Environ.* **408**, 4749-4760 (2010).
- 442 34. Wortmann, M. Hydrological modelling of the Lena River using SWIM (Potsdam
443 Institute for Climate Impact Research, Germany, 2014).
- 444 35. Yu, S., et al. Impacts of anthropogenic activities on weathering and carbon fluxes:
445 a case study in the Xijiang River basin, southwest China. *Environ. Earth Sci.* **75**,
446 11 (2016).
- 447 36. Zhang, S. R., et al. Water chemistry of the Zhujiang (Pearl River): Natural
448 processes and anthropogenic influences. *J. Geophys. Res.-Earth Surf.* **112**, 17
449 (2007).
- 450 37. Zhulidov, A., et al. Long-term dynamics of water-borne nitrogen, phosphorus and
451 suspended solids in the lower Don River basin (Russian Federation). *J. Water Clim.*
452 *Chang.* **2**, 201-211 (2011).
- 453 38. Xia, X. H. Water quality (major ions) evolution of the Yangtze river system from
454 1960's to 1990's (Peking University, Beijing, 1998). in Chinese.
- 455 39. Grubbs, F. E. Sample criteria for testing outlying observations. *Ann. Math. Stat.* **21**,
456 27-58 (1950).
- 457 40. Howell, D. C. Statistical methods in human sciences (Wadsworth, New York, 1998).
- 458 41. Wang, J. Contribution of Upstream Tributaries and Returned Irrigation
459 Groundwater to Chemical Weathering in the Yellow River Basin (Ocean University
460 of China, Qingdao, 2014). in Chinese.

- 461 42. Jacobson, A. D. & Blum, J. D. Relationship between mechanical erosion and
462 atmospheric CO₂ consumption in the New Zealand Southern Alps. *Geology* **31**,
463 865-868 (2003).
- 464 43. Runkel, R. L., Crawford, C. G. & Cohn, T. A. Load Estimator (LOADEST): A
465 FORTRAN program for estimating constituent loads in streams and rivers (U. S.
466 Geological, Virginia, 2004).
- 467 44. Burnham, K. P. & Anderson, D. R. Model Selection and Multi- Model Inference: a
468 Practical Information-Theoretic Approach (Springer-Verlag, New York, 2002).
- 469 45. Meybeck, M., Durr, H. H. & Vörösmarty, C. J. Global coastal segmentation and its
470 river catchment contributors: A new look at land-ocean linkage. *Global*
471 *Biogeochem. Cycles* **20**, 1-15 (2006).
- 472 46. Durr, H. H., Meybeck, M., Hartmann, J., Laruelle, G. G. & Roubeyx, V. Global
473 spatial distribution of natural riverine silica inputs to the coastal zone.
474 *Biogeosciences* **8**, 597-620 (2011).
- 475 47. Fekete, B. M., Vörösmarty, C. J. & Grabs, W. High-resolution fields of global
476 runoff combining observed river discharge and simulated water balances. *Global*
477 *Biogeochem. Cycles* **16**, 1-11 (2002).
- 478 48. Meybeck, M. & Ragu, A. River discharges to the oceans: an assessment of
479 suspended solids, major ions and nutrients (United Nations Environment
480 Programme, Paris, 1995).
- 481 49. Mann, H. B. Nonparametric test against trend. *Econometrica* **13**, 245-259 (1945).
- 482 50. Kendall, M. Rank correlation measures (Charles Griffin, London, 1976).

- 483 51. Yue, S., Pilon, P., Phinney, B. & Cavadias, G. The influence of autocorrelation on
484 the ability to detect trend in hydrological series. *Hydrol. Processes* **16**, 1807-1829
485 (2002).
- 486 52. Meybeck, M. Global Occurrence of Major Elements in Rivers. *Treatise Geochem.*
487 **5**, 207-223 (2003).
- 488 53. Drake, T. W., et al. Increasing Alkalinity Export from Large Russian Arctic Rivers.
489 *Environ. Sci. Technol.* **52**, 8302-8308 (2018).
- 490 54. Global Environment Monitoring System for Water. Global Water Quality database.
491 <https://gemstat.org> (2018).
- 492 55. McGowan, W. Water processing: residential, commercial, light-industrial 3rd edn
493 (Water Quality Association, Lisle, 2000).
- 494 56. Do, H. X., Gudmundsson, L., Leonard, M. & Westra, S. The Global Streamflow
495 Indices and Metadata Archive (GSIM) - Part 1: The production of a daily
496 streamflow archive and metadata. *Earth Syst. Sci. Data* **10**, 1-21 (2018).
- 497 57. Bai, R., Li, T., Huang, Y., Li, J. & Wang, G. An efficient and comprehensive method
498 for drainage network extraction from DEM with billions of pixels using a size-
499 balanced binary search tree. *Geomorphology* **238**, 56-67 (2015).
- 500 58. Hartmann, J. & Moosdorf, N. The new global lithological map database GLiM: A
501 representation of rock properties at the Earth surface. *Geochem., Geophys., Geosyst.*
502 **13**, 1-37 (2012).
- 503 59. Rubel, F. & Kotteck, M. Observed and projected climate shifts 1901–2100 depicted
504 by world maps of the Köppen-Geiger climate classification. *Meteorol. Z.* **19**, 135-

- 505 141 (2010).
- 506 60. Peel, M. C., Finlayson, B. L. & McMahon, T. A. Updated world map of the
507 Köppen-Geiger climate classification. *Hydrol. Earth Syst. Sci.* **11**, 1633-1644
508 (2007).
- 509 61. Tateishi, R., et al. Production of global land cover data – GLCNMO. *Int. J. Digit.*
510 *Earth* **4**, 22-49 (2011).
- 511 62. Siebert, S., Henrich, V., Frenken, K. & Burke., J. Global Map of Irrigation Areas
512 version 5. [http://www.fao.org/aquastat/en/geospatial-information/global-maps-](http://www.fao.org/aquastat/en/geospatial-information/global-maps-irrigated-areas/latest-version)
513 [irrigated-areas/latest-version](http://www.fao.org/aquastat/en/geospatial-information/global-maps-irrigated-areas/latest-version) (2019).
- 514 63. Lehner, B., et al. High-resolution mapping of the world's reservoirs and dams for
515 sustainable river-flow management. *Front. Ecol. Environ.* **9**, 494-502 (2011).
- 516 64. Center for International Earth Science Information Network. Documentation for
517 the Gridded Population of the World, Version 4 (GPWv4).
518 <http://dx.doi.org/10.7927/H4D50JX4> (2016).
- 519 65. Laraque, A., et al. A comparison of the suspended and dissolved matter dynamics
520 of two large inter-tropical rivers draining into the Atlantic Ocean: the Congo and
521 the Orinoco. *Hydrol. Processes* **27**, 2153-2170 (2013).
- 522 66. Samba, G., Nganga, D. & Mpounza, M. Rainfall and temperature variations over
523 Congo-Brazzaville between 1950 and 1998. *Theor. Appl. Climatol.* **91**, 85-97
524 (2008).
- 525 67. Mosley, L. M., et al. The impact of extreme low flows on the water quality of the
526 Lower Murray River and Lakes (South Australia). *Water Resour. Manage.* **26**,

- 527 3923-3946 (2012).
- 528 68. Potter, N. J. & Chiew, F. H. S. An investigation into changes in climate
529 characteristics causing the recent very low runoff in the southern Murray-Darling
530 Basin using rainfall-runoff models. *Water Resour. Res.* **47**, 1-12 (2011).
- 531 69. Chiew, F. H. S. & McMahon, T. A. Groundwater recharge from rainfall and
532 irrigation in the Campaspe River Basin. *Aust. J. Soil Res.* **29**, 651-670 (1991).
- 533 70. Chen, J. S. River water quality in China (Science Press, Beijing, 2006). in Chinese.
- 534 71. Milliman, J. D. & Farnsworth, K. L. River discharge to the coastal ocean: a global
535 synthesis (Cambridge University Press, New York, 2011).
- 536 72. Barles, S. Urban metabolism and river systems: an historical perspective - Paris
537 and the Seine, 1790-1970. *Hydrol. Earth Syst. Sci.* **11**, 1757-1769 (2007).
- 538 73. Morford, S. L. Salinity in the Colorado River Basin.
539 [https://watershed.ucdavis.edu/education/classes/files/content/page/6%20Morford-](https://watershed.ucdavis.edu/education/classes/files/content/page/6%20Morford-Colorado_Basin_Salinity.pdf)
540 [Colorado_Basin_Salinity.pdf](https://watershed.ucdavis.edu/education/classes/files/content/page/6%20Morford-Colorado_Basin_Salinity.pdf) (2014).
- 541 74. McCabe, G. J., Wolock, D. M., Pederson, G. T., Woodhouse, C. A. & McAfee, S.
542 Evidence that Recent Warming is Reducing Upper Colorado River Flows. *Earth*
543 *Interact.* **21**, 1-14 (2017).
- 544 75. Udall, B. & Overpeck, J. The twenty-first century Colorado River hot drought and
545 implications for the future. *Water Resour. Res.* **53**, 2404-2418 (2017).
- 546 76. Maupin, M. A., Ivahnenko, T. I. & Bruce, B. Scientific Investigations Report:
547 Estimates of water use and trends in the Colorado River Basin, Southwestern
548 United States, 1985–2010 (U. S. Geological Survey, Reston, 2018).

- 549 77. Farinosi, F., et al. Future Climate and Land Use Change Impacts on River Flows in
550 the Tapajós Basin in the Brazilian Amazon. *Earth's Future* **7**, 993-1017 (2019).
- 551 78. Pantoja, N. G. P., et al. Quality of the Solimoes River water for domestic use by
552 the riverine community situated in Manacapuru-Amazonas-Brazil. *Environ. Sci.*
553 *Pollut. Res.* **23**, 11395-11404 (2016).
- 554 79. Shiklomanov, A. I. & Lammers, R. B. River ice responses to a warming Arctic-
555 recent evidence from Russian rivers. *Environ. Res. Lett.* **9**, 1-9 (2014).
- 556 80. Smith, L. C. Trends in Russian Arctic river-ice formation and breakup, 1917 to
557 1994. *Phys. Geogr.* **21**, 46-56 (2000).
- 558 81. Pokrovsky, O. S., et al. Biogeochemistry of carbon, major and trace elements in
559 watersheds of northern Eurasia drained to the Arctic Ocean: The change of fluxes,
560 sources and mechanisms under the climate warming prospective. *C. R. Geosci.* **344**,
561 663-677 (2012).
- 562 82. Viers, J., et al. Seasonal and spatial variability of elemental concentrations in boreal
563 forest larch foliage of Central Siberia on continuous permafrost. *Biogeochemistry*
564 **113**, 435-449 (2013).
- 565 83. Miao, C. Y., Ni, J. R., Borthwick, A. G. L. & Yang, L. A preliminary estimate of
566 human and natural contributions to the changes in water discharge and sediment
567 load in the Yellow River. *Global Planet. Change* **76**, 196-205 (2011).
- 568 84. Zhang, Y. K. & Schilling, K. E. Increasing streamflow and baseflow in Mississippi
569 River since the 1940 s: Effect of land use change. *J. Hydrol.* **324**, 412-422 (2006).
- 570 85. Kaushal, S. S., et al. Freshwater salinization syndrome on a continental scale. *Proc.*

- 571 *Natl. Acad. Sci. U. S. A.* **115**, E574-E583 (2018).
- 572 86. Sarin, M. M., Krishnaswami, S., Dilli, K., Somayajulu, B. L. K. & Moore, W. S.
573 Major ion chemistry of the Ganga-Brahmaputra river system: Weathering
574 processes and fluxes to the Bay of Bengal. *Geochim. Cosmochim. Acta* **53**, 997-
575 1009 (1989).
- 576 87. Galy, A. & France L. C. Weathering processes in the Ganges-Brahmaputra basin
577 and the riverine alkalinity budget. *Chem. Geol.* **159**, 31-60 (1999).